

Enhanced Thermoelectric Properties of 2D Janus Ferromagnetic LaBrI with Strain-induced Valley Degeneracy

Anuja Kumari,^{1, a} Abhinav Nag,² Santanu K. Maiti,^{1, b} Jagdish Kumar^{3, 4}

¹Physics and Applied Mathematics Unit, Indian Statistical Institute, 203 Barrackpore Trunk Road, Kolkata-700 108, India

²Department of Physics, GGSDS college, Rajpur, Palampur-176061, India

³Department of Computational Sciences, Central University of Punjab, Bhatinda-151 401, India

⁴Department of Physics, Central University of Himachal Pradesh, Dharamshala-176 215, India

^aanudhiman45@gmail.com

^bsantanu.maiti@isical.ac.in

Since the successful synthesis of the MoSSe monolayer, which violated the out-of-plane mirror symmetry of TMDs monolayers, considerable and systematic research has been conducted on Janus monolayer materials. By systematically analyzing the LaBrI monolayer, we are able to learn more about the novel Janus material by focusing on the halogen family next to group VIA (S, Se, Te). The structural optimizations have been carried out using the FP-LAPW (Full Potential Linear Augmented Plane Wave) basis, as implemented in the ELK using tb-mBJ exchange correlation potential. Computed structural parameters are in good comparison with literature reports. Further, optimized crystal structures were used for computing effect of strain on electronic and thermoelectric properties using pseudo potential based Quantum espresso code. Dynamical stability predicts material can withstand strain upto 10% strain. Computed electronic structure reveals material to be indirect wide bandgap ferromagnetic material with magnetic moment $1\mu_B$. With increase in the biaxial tensile strain the band gap increases. Furthermore, the computed magneto-thermoelectric properties predicts high Seebeck coefficient of $\sim 400 \mu\text{V/K}$ and low thermal conductivity of $\sim 1.13 \times 10^{14} \text{ W/msK}$ in LaBrI which results high ZT of ~ 1.92 with 8% strain at 800 K with p-type doping. Thus, present study supports the fact that tensile strain on ferromagnetic LaBrI material can further enhance TE properties and making it to be a promising material for TE applications at higher temperature.

Keywords: Density functional theory, Tran-Blaha exchange potential, magneto-thermoelectric properties, Figure of merit.

1. Introduction

Clean energy sources and renewable energy technology are the utmost priority of scientists, ecologists and researchers to combat global warming and climate change [1]-[5]. Among various factors, waste heat is one of the prime concerns causing it. By scavenging wasted heat, we can save energy and promote energy production [6]-[11]. Thus, it is significant to explore new ways to generate, convert, and store energy. Thermoelectric generators (TEGs) are a highly effective solution in managing waste heat as they can convert waste thermal heat into useful electrical energy [12]-[16]. TEGs are significantly known for their applications in deep space exploration because of immobile parts, silent working, and steadiness during years of

operation. A thermoelectric module is simply composed of parallel thermal and series electrical connections between pairs of highly doped p-type and n-type semiconductors. For any good TE module, these p-type and n-type TE materials are very crucial. Thus, researchers have explored many different TE materials for power generation at various temperatures. Although conversion efficiency is not yet achieved for commercialization of this technology and is yet a challenge [17]-[20]. The efficiency of any thermoelectric material is assessed by a dimensionless parameter called a figure of merit denoted by ZT as [21],[22]

$$ZT = \frac{S^2 \sigma T}{K}. \quad 1.1$$

In the above equation, S represents the Seebeck coefficient, σ represents the electrical conductivity, and K represents thermal conductivity. Thus, a factor known as the power factor, $S^2\sigma$, indicates the electric performance of the material. Also, the total thermal conductivity K comprises of electronic thermal conductivity K_e and phononic thermal conductivity K_l . For high ZT or to achieve optimal thermal performance at a certain temperature, a higher power factor and lower thermal conductivity are essential [23]-[26]. However, for any given material three parameters S , σ , and K_e are coupled together, and optimizing them simultaneously is a daunting task [27]-[32]. This unveils various strategies to improve (TE) materials such as power factor augmentation by carrier filtering [33]-[37], carrier pocket engineering [38]-[40], complex structures [41]-[42], low dimensional structures [43]-[45] and valley degeneracy[46] etc., that improves ZT significantly. Also, improved phonon scattering using nano-structuring has been used to raise the TE material's energy conversion efficiency [47].

With the prediction of excellent transport properties and large power factors of graphene [48] and layered materials [49]-[52], many 2D materials were investigated for thermoelectric applications. Due to their indifferent structural, physical, and chemical properties and easy synthesis using a variety of methods such as Chemical vapor deposition (CVD), physical vapor deposition, mechanical exfoliation etc., they are of recent interest in thermoelectric [53]-[56]. Gu and Yang [57] predicted that altering the stoichiometry of the structure can lead to a significant reduction in the lattice thermal conductivity. The ZT can be efficiently increased by low lattice thermal conductivity. Recently, the synthesis of Janus MoSSe monolayer [58] inspired the research community to explore a new family of 2D materials named Janus materials. Due to

highly asymmetric structural characteristics, Janus materials exhibit diverse and fascinating properties, including finite out-of-plane dipoles, giant Rashba splitting, a wide range of direct and indirect band gaps, etc. In Janus transition metal dichalcogenides (TMDCs) monolayer, the layer of metal atoms is sandwiched between two layers of dissimilar chalcogen atoms. They possess an extra degree of freedom to tune material properties while retaining the exotic characteristics of their parent structure. Numerous works in the literature suggested that these Janus materials can be a potential material for TE applications. Furthermore, recent theoretical studies suggest that the Janus monolayer can be useful in a variety of emerging fields [59]. For thermoelectric application, study by Abhishek *et al.*[60] reported a high ZT of 2.56 for the WSTe Janus monolayer at higher temperature, another Janus monolayer ZrSSe studied by S. Zhao *et al.* [61] have shown high ZT of 4.41 and 4.88 for p-type and n-type materials with a tensile strain of 6%. Similarly, ZT of 2.54 for PtSeTe Janus monolayer is observed at 900K by Wang *et al.* [62] and ZT of ~ 3 is reported by Shivani *et al.*[63] in MoSSe Janus monolayer at 1200K.

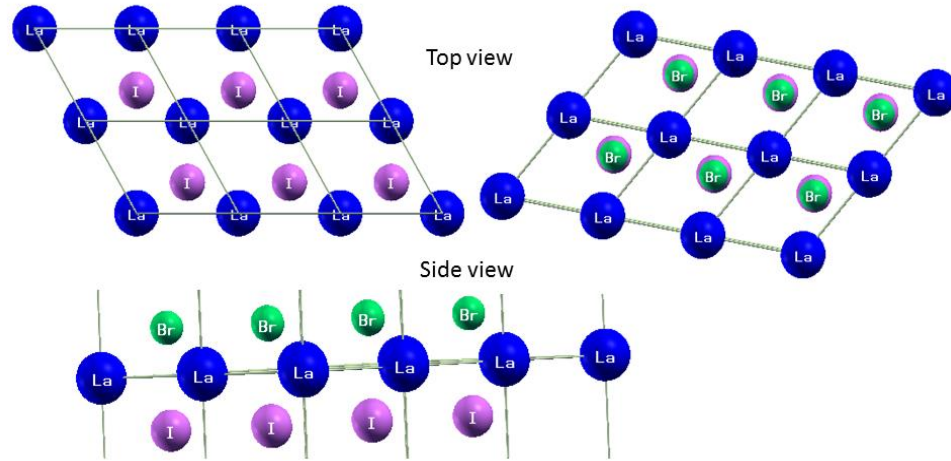


Figure 1: Crystal structure of 2D Janus monolayer of LaBrI (P3m1: no. 156) top view and side view.

Some magnetic Janus materials were also recently proposed such as manganese chalcogenides [64] and chromium trihalides [65]. Similarly, P. Jiang and Lili Kang predicted a 2D magnetic Janus ferrowalley material LaBrI to be a stable ferromagnetic electrode [66] from the first principle study. They proposed that the intrinsic magnetism and asymmetric nature of these materials result in large valley degeneracy and hence making these materials a promising material for various applications. Interestingly, due to valley degeneracy, the WSSe Janus

monolayer shows good thermoelectric properties [67]. Motivated by their idea, we have investigated various properties of 2D magnetic Janus material LaBrI for thermoelectric applications. Janus monolayer of LaBrI has broken out-of-plane symmetry from D_{3h} (LaBr₂) to C_{3v} (LaBrI) with space group P3m1 (No. 156) as shown in Figure 1. This monolayer is a three-atomic thick layered structure with Li atoms sandwiched between two halogen atoms Br and I having reflection asymmetry on the mirror plane.

In the present study, we have systematically investigated the structural properties, dynamical stability, electronic properties, and thermoelectric properties of this material. To the best of our knowledge, a study on the thermoelectric properties of this material was not reported yet. Furthermore, we present modulated ferrovalley for up-spin and down-spin-charge carriers in electronic band structure which further increases with an increase in strain. Due to this modulation in valley degeneracy low thermal conductivity is observed which enhances the figure of merit ZT to >1 . Thermoelectric coefficients as a function of chemical potential at various temperatures predict $ZT >1$ with p-type and n-type doping at different temperatures. Obtained low thermal conductivity and high ZT values tuned with strain are the essential findings of our study that predicts this material to be an efficient thermoelectric element.

The present paper is arranged as follows: In Sec. 2 we discuss the theoretical formalism of DFT used in computing all the calculations. In Sec. 3 we further present and discuss lattice parameters, dynamical stability based on phonon dispersion curves and various thermoelectric parameters such as the Seebeck coefficient, electrical conductivity, power factor and ZT of the material finally in Sec. 4 we conclude with significant outcomes of present study.

2. Computational Details

All the calculations were carried out in the framework of the density functional theory (DFT) based formalisms. Janus monolayer of LaBrI is designed from pristine LaBr₂ monolayer by replacing Br atoms with Iodine atoms. We have optimized the obtained Janus monolayer using full potential linear augmented plane wave (FP-LAPW) formalism as implemented in Elk code [68]. Using the optimized lattice parameters, the calculations of electronic and dynamical properties have been further carried out in pseudo-potential-based Quantum espresso code [69]. The exchange and correlation interaction among the electrons are described using the non-

empirical *generalized gradient approximation* within the framework of PBE formalism which performs reasonably accurate for a wide range of materials [70]. We have used a plane-wave basis set energy cutoff of 350 eV and for sampling the Brillouin zone (BZ) the Monkhorst-Pack of $12 \times 12 \times 1$ k -points for electronic properties and $36 \times 36 \times 2$ for thermoelectric properties are used. The lattice parameters and atomic positions were obtained by relaxing the structures to force tolerance of 10^{-4} eV/atom. A large vacuum space of 15 Å is used along the z-axis to prevent any artificial interactions between periodic images of slabs along the vertical direction. The phonon dispersion calculations were employed for the dynamical stability. The electronic thermoelectric coefficients were computed using the semi-classical Boltzmann transport theory within constant scattering time (CSTA) and the rigid band approximations, as implemented in the BoltzTrap code [71]. According to semi-classical Boltzmann transport theory, once we get the first principle band structure calculations we can define *Energy projected conductivity tensor* ' $\Theta(\varepsilon)$ ' in terms of conductivity tensor as

$$\Theta(\varepsilon) = \frac{1}{N} \sum_k \sigma(k) \left(-\frac{\delta(\varepsilon - \varepsilon_k)}{d\varepsilon} \right) . \quad 2.1$$

It shows the distribution in energy and represents the contribution of electrons having a specific energy ' ε ' and ' N ' represents the number of k -points sampled in the Brillouin zone. For a unit cell crystal having volume Ω , the transport coefficients can be evaluated by integrating this conductivity distribution as;

$$\sigma(T, \mu) = \frac{1}{\Omega} \int \Theta(\varepsilon) \left[-\frac{\delta f_\mu(T, \varepsilon)}{\delta k} \right] d\varepsilon , \quad 2.2$$

$$\kappa_e(T, \mu) = \frac{1}{eT\Omega} \int \Theta(\varepsilon) (\varepsilon - \mu)^2 \left[\frac{\delta f_\mu(T, \varepsilon)}{\delta k} \right] d\varepsilon , \quad 2.3$$

$$S(T, \mu) = \frac{1}{eT\Omega T(T, \mu)} \int \Theta(\varepsilon) (\varepsilon - \mu) \left[\frac{\delta f_\mu(T, \varepsilon)}{\delta k} \right] d\varepsilon . \quad 2.4$$

Where, T is the equilibrium temperature, μ is the chemical potential, κ_e is the electronic part of the thermal conductivity and S refers to the Seebeck coefficient. Finally, the figure of merit (ZT) can be obtained by,

$$ZT = \frac{S^2 \sigma T}{\kappa_e + \kappa_l}.$$

Here, ZT represents the heat to electrical energy conversion efficiency. To obtain more accurate value of ZT, phonon contribution towards thermal conductivity is required, but as the literature suggests that strain mediated valley degeneracy reduces thermal conductivity significantly [67], the phonon contribution becomes negligibly small and thus straightaway we ignore this part in our calculations, without loss of any generality.

3. Results and Discussion

3.1 Structural properties

By allowing the crystal to relax to a force tolerance of 0.001eV/atom, the equilibrium lattice parameters for all the compositions under investigation have been determined. Using the Tran Blaha modified Becke Johnson as the exchange-correlation, we are able to calculate the lattice constants and other related parameters that are listed in Table 1. These data match well with the previous estimates [66].

Table 1: Lattice constants and bandgap of various strains on Janus LaBrI systems obtained using TbmBJ exchange and correlation for electrons.

S. No.	Compressive biaxial tensile strain	Parameter	LaBrI
1	0%	Lattice constant (Å)	4.49 (4.24)[66]
		Bandgap (eV)	2.19eV (↑spin) 1.15eV (↓spin)
2	6%	Lattice constant (Å)	4.76
		Bandgap (eV)	1.53eV (↑spin) 0.56eV (↓spin)
3	10%	Lattice constant (Å)	4.94
		Bandgap (eV)	1.67eV (↑spin) 0.58eV (↓spin)

3.2 Lattice Dynamics and Dynamical Stability

The thermoelectric performance of a material drastically changes with the implication of strain (ϵ). The tensile strain is defined as $\epsilon \% = \left(\frac{a-a_0}{a_0}\right) \times 100$ where a_0 is the equilibrium relaxed lattice constant. We examined the effect of biaxial tensile strain on the dynamical

stability of LaBrI by calculating phonon dispersion curves at the steps of $\Delta\varepsilon=2\%$. Figure 2, illustrates the phonon dispersions at various strains for LaBrI Janus monolayers along different high-symmetry directions.

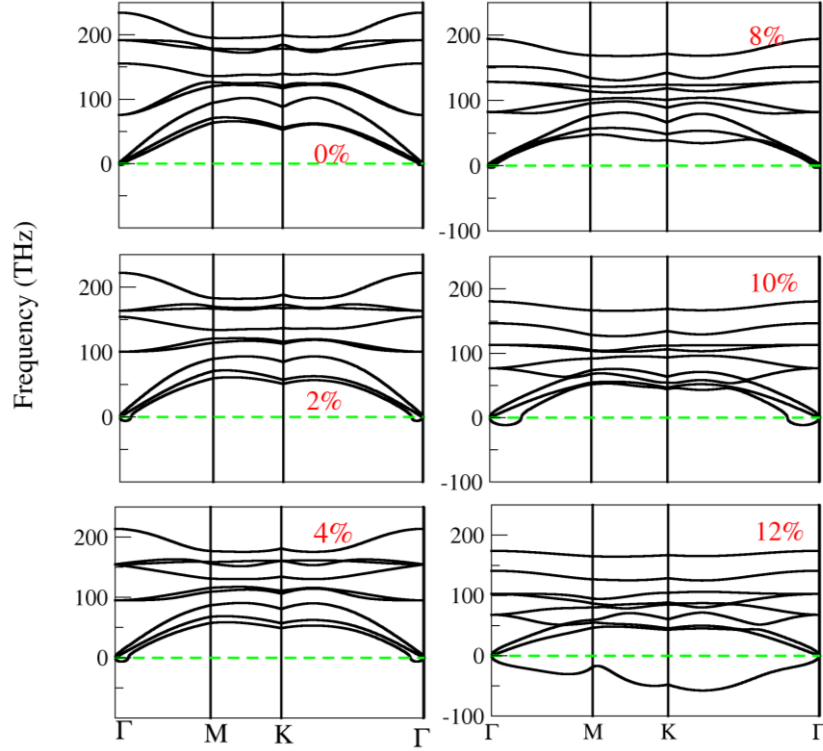


Figure 2: Phonon dispersion for LaBrI at different biaxial tensile strain with $\Delta\varepsilon=2\%$ along high symmetry k-points.

The computed phonon dispersion for LaBrI comprises three acoustic and six optical branches in the dispersion curves which is due to the one Li atom, one Br atom, and one I atom in the unit cell. The phonon dispersion curve relates the dependence of phonon frequencies for all branches along selected high symmetry path. The dynamical stability of a material is associated with the real and imaginary frequencies of the phonon dispersion curves. An imaginary frequency in the phonon curve signifies the non-restorative force which results in the decrease in potential energy of the atoms when displaced from equilibrium positions and thus making it unstable. Computed phonon dispersion curves for LaBrI do not contain any imaginary phonon frequencies up to 10%. This indicates that this monolayer is dynamically stable under tensile strain up to 10%. Further increase in the strain led to imaginary frequencies in the phonon dispersion curve and hence material gets unstable beyond this limit.

3.3 Electronic Properties

The electronic band structure and total density of states (TDOS) for the studied materials are shown in Fig. 3. Band structures in Fig. 3 highlight that GGA-PBE predicts LaBrI to be a semiconductor with an indirect band gap of 0.537 eV which supports the literature report [66] as 1.02 eV. It can be seen from Fig. 3 that near the Fermi level up spin and down spin carriers are significant for 0% strain. LaBrI is a ferromagnetic material with a magnetic moment of $1\mu_B$. Whereas with an increase in strain, this transition vanishes and only down spin carriers are contributing.

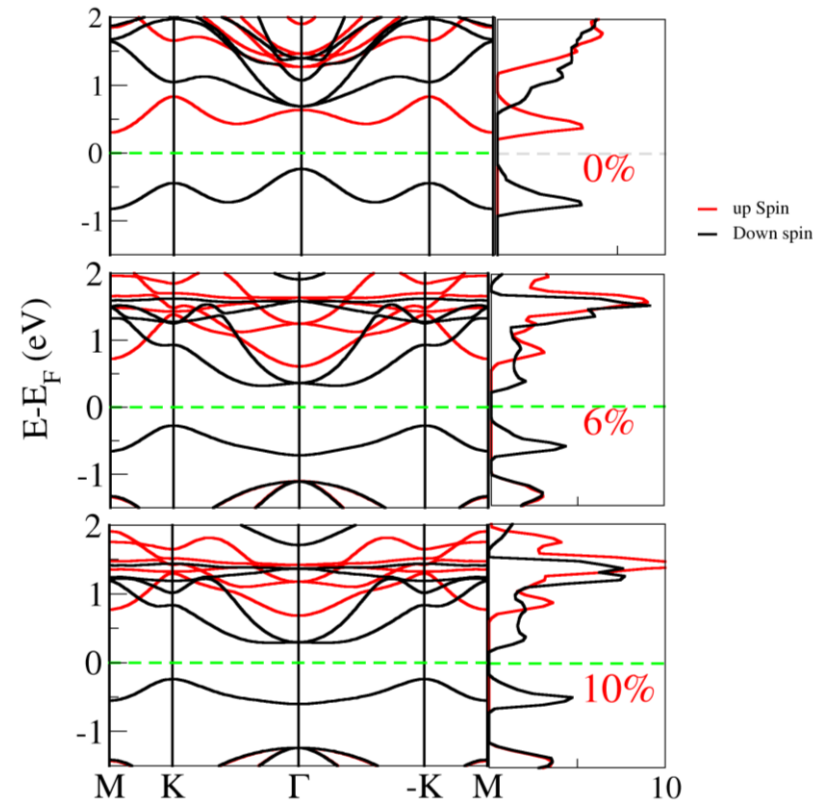


Figure 3: Electronic band structure on the left-hand side and TDOS plot on the right-hand side obtained using TbmBJ for various strains on LaBrI.

It is apparent from Fig. 3, that LaBrI shows an indirect band gap from Γ to M k-point. We observed significant changes in the conduction band region when a tensile strain is applied to the material. The energies at both the Γ and M points increase as the strain increases and the energy at Γ point shifts slower than that at M point. With the increase in strain the bandgap increases. This can be realized as when strain is applied, the bonds are either stretched or compressed and

thus there is some limit the bond can sustain or else it breaks. When we apply tensile strain, the bond is stretched which results in a change in the separation of the respective atoms. Thus, with increase in the separation of the system the energy of the system enhances and hence the band gap widens with the upsurge in the applied strain. We found that when a biaxial strain is applied, the band valleys in these Janus monolayers can be significantly tuned to open up an indirect band gap. This opening up of the bandgap can lead to a significant effect on the thermoelectric properties. It can be observed that the strain also has a significant effect on the band curvatures and hence the effective mass of the charge carriers in valance and conduction bands.

3.3 Thermoelectric Properties

The electronic thermoelectric coefficients of the considered monolayer have been computed which include the Seebeck coefficient (S), electrical conductivity (σ), electronic part of thermal conductivity (κ_e) and power factor $S^2\sigma$ by solving the Boltzmann transport equations within constant scattering time approximation (CSTA) and rigid band assumption. We have investigated the impact of doping the charge carriers on the transport coefficients by varying the chemical potential (μ). The transport properties are significantly dependent on the location of the chemical potential. The negative and positive doping levels of the chemical potential refer to electron (n -type) and hole (p -type) dopings, respectively.

3.3.1 Seebeck coefficient (S)

The Seebeck coefficient is the induced electric potential due to thermal gradient across a thermocouple. Therefore, a higher Seebeck coefficient signifies higher electric potential across thermal gradient and is essential for higher ZT or good thermoelectric material. For a given material, the Seebeck coefficient is related to carrier concentration ' n ' as [72],[73]

$$S = \frac{8\pi^2 k_B^2 T}{3eh^2} m^* \left(\frac{\pi}{3n}\right)^{\frac{2}{3}} \quad 3.1$$

where, T is the temperature, k_B is Boltzmann's constant, e is electronic charge, m^* is effective mass, and h is Planck constant. Within constant scattering time approximation (CSTA) the electronic conductivity tensor $\Xi(\epsilon)$ as discussed in Sec. 2, can be obtained only from the velocities that follow electronic band structure. The chemical potential μ is used as a variable parameter to study the effect of doping. The obtained Seebeck coefficient for the monolayer of LaBrI as a function of carrier concentration is depicted in Fig. 4. For unstrained monolayer, the

highest Seebeck coefficient of $\sim 466\mu\text{V/K}$ is obtained at 600K for up spin-charge carriers, while for down spin-charge carriers temperature does not have a significant effect and a coefficient of $\sim 112\mu\text{V/K}$ was recorded with positive doping levels. The Seebeck coefficients for different biaxial tensile strains at various temperatures 600K, 800K, 1200K and 1500K are also illustrated in these plots. For spin-up charge carriers Seebeck coefficient decreases to $\sim 330\mu\text{V/K}$ with strain and similar trends are observed with an increase in temperature. However, for down spin charge carriers it increases to $\sim 480\mu\text{V/K}$ with positive doping levels at 600K. At higher temperatures 1200K and 1500K, we get a significantly low value of the Seebeck coefficients.

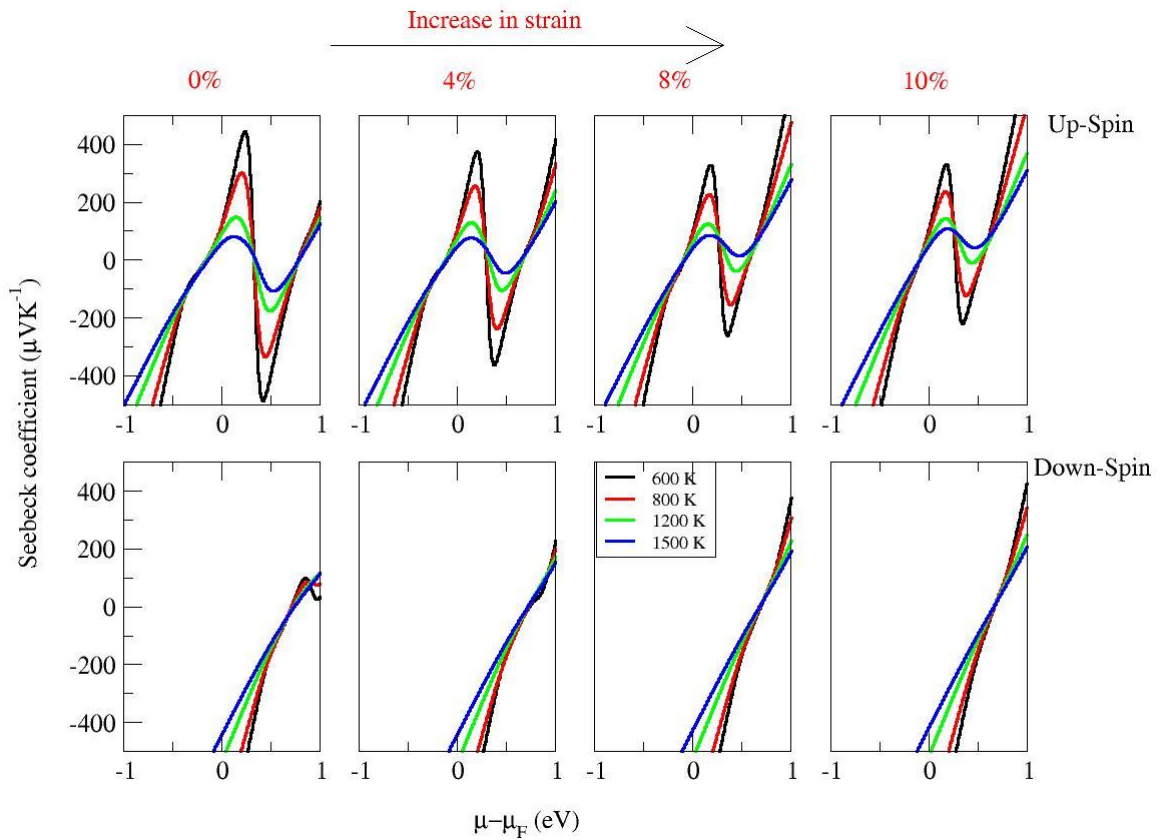


Figure 4: Seebeck coefficient as a function of chemical potential at 600K, 800K, 1200K, and 1500K for spin-up and spin-down charge carriers.

3.3.3 Thermal conductivity (K)

To obtain an optimization between electronic conductivity and thermal conductivity we need to understand the relation among them. At an absolute temperature, they are related by Wiedemann-Franz law as $\frac{\kappa_e}{\sigma} = LT$ [74], where (κ_e) is the electronic thermal conductivity, (σ) is the electrical conductivity, L is the Lorenz number and T is the absolute temperature. According

to this law that refers to the simplest free electron model, the electrical and thermal conductivities should be in direct relation to get the Lorenz number as a constant at a particular temperature. However, in a more realistic scenario of complex interactions within the crystal structure, we can find a way to optimize the thermoelectric performance of any material.

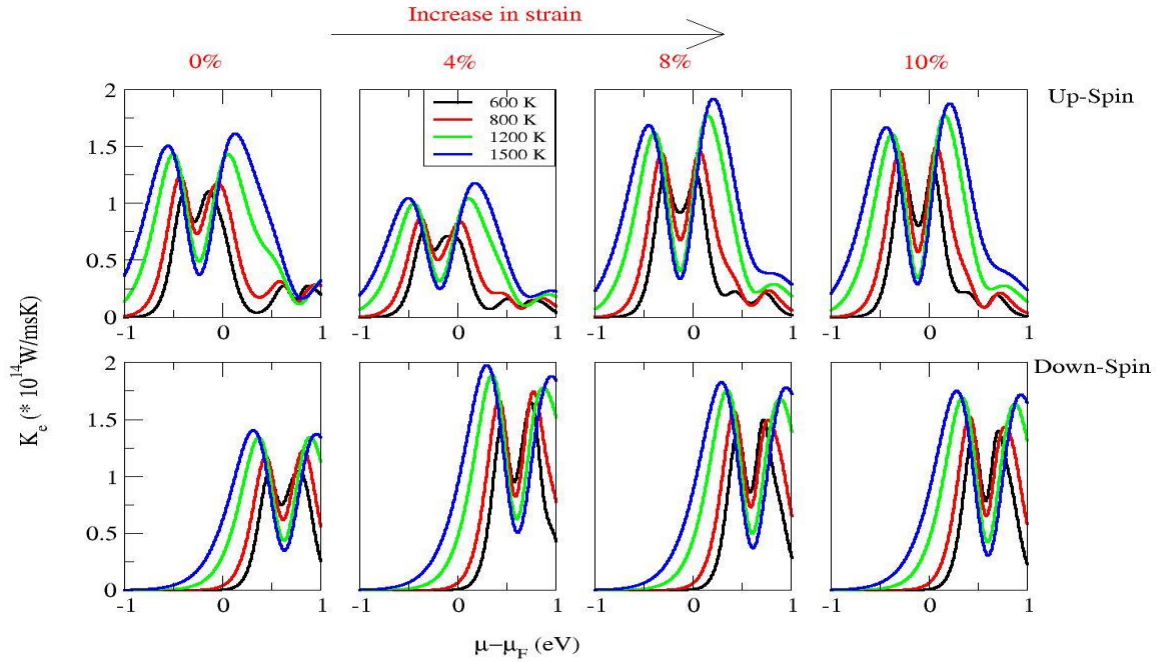


Figure 5: Variation of electronic part of thermal conductivity with chemical potential at various temperature regions for spin up and down spin charge carriers.

Figure 5 depicts the electronic thermal conductivity of this monolayer for *n*- and *p*-type dopings at different temperatures. It can be observed from the plots that in an unstrained system, spin-up and spin-down charge carriers have a lower thermal conductivity of $\sim 1.14 \times 10^{14} W/mKs$ and $\sim 1.02 \times 10^{14} W/mKs$ at 600K respectively. With further increase in temperature to 1500K it increases to $\sim 1.68 \times 10^{14} W/mKs$ and $\sim 1.39 \times 10^{14} W/mKs$. However, the increase in strain has prominent changes in both spin up and spin down charge carriers as with 4% strain, the thermal conductivity decreases to $\sim 0.62 \times 10^{14} W/mKs$ for spin up and it increases to $\sim 1.64 \times 10^{14} W/mKs$ for spin down charge carriers at 600K. A similar trend is observed concerning increase in temperature respectively. With further increase in strain increases the thermal conductivity to $\sim 1.88 \times 10^{14} W/mKs$ for both spin up and spin down charge carriers at 1500K. Therefore, overall the tensile strain seems to be favorable for enhancing the thermoelectric performance of this monolayer.

3.3.4 Power Factor ($S^2\sigma$)

The ZT of any TE material is directly proportional to its power factor which is defined as $PF = S^2\sigma$. It significantly comprises of the electronic conductivity and Seebeck coefficient.

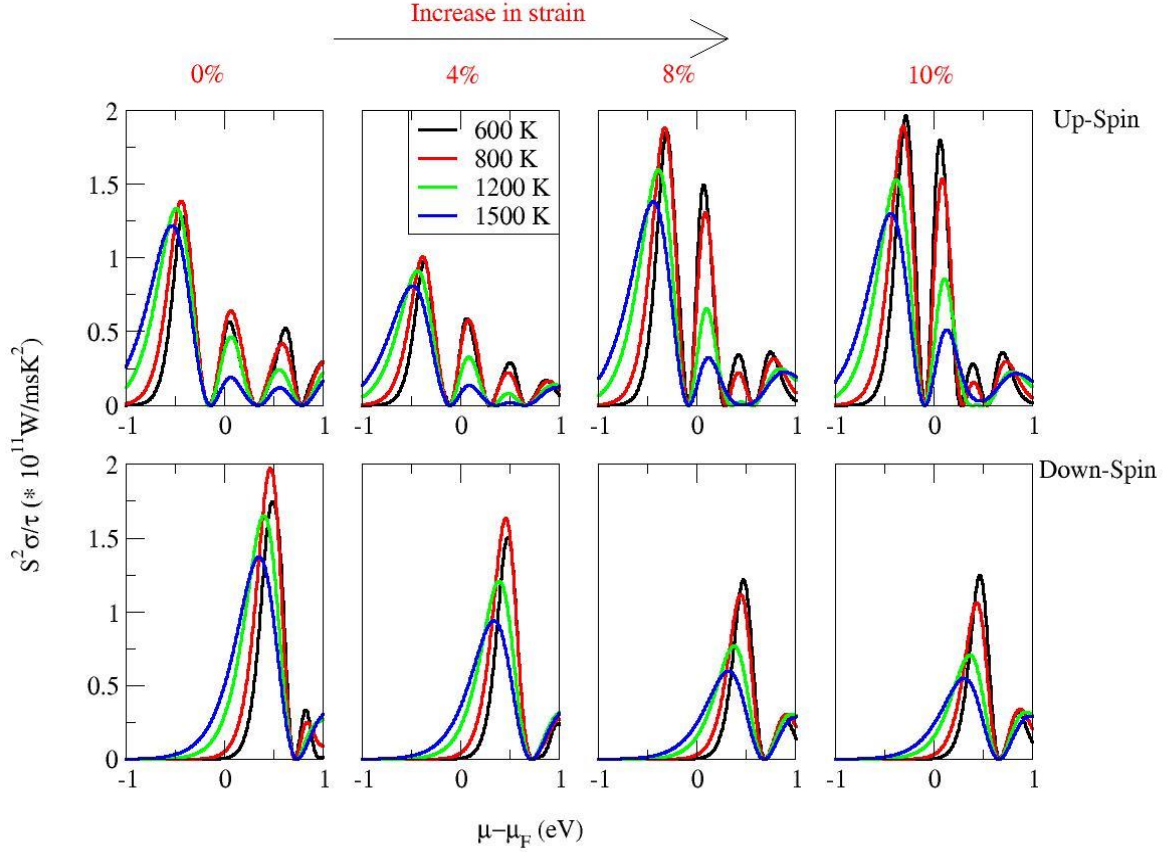


Figure 6: Spin resolved power factor as a function of chemical potential at 600K, 800K, 1200K and 1500K.

Figure 6 illustrates calculated power factor as a function of chemical potential employed at different strain under various temperature. For unstrained LaBrI, spin up charge carriers show decrease in PF from $\sim 1.28 \times 10^{11} W/mK$ at 600K to $\sim 1.16 \times 10^{11} W/mK$ at 1500K and spin down charge carriers shows increase in PF from $\sim 1.78 \times 10^{11} W/mK$ at 600K to $\sim 1.96 \times 10^{11} W/mK$ at 800K. Further, at 800K with 8% strain, spin up carriers shows PF $\sim 1.83 \times 10^{11} W/mK$ with n-type doping and spin down charge carriers show lower PF $\sim 1.04 \times 10^{11} W/mK$ with p-type doping. At high temperatures, we can observe decrease in the power factor. Thus, strain significantly enhances the band curvatures and hence the relevant effect can be seen in the power factor for up spin and down spin charge carriers.

3.3.5 Thermoelectric Figure of Merit (ZT)

We calculate the dimensionless figure of merit to predict the thermoelectric efficiency. Interestingly, computed results for unstrained LaBrI have $ZT < 1$ without doping and $ZT > 1$ for n-type and p-type dopings for both spins. Variations of temperature and strain have significant effect on ZT. At 600K, ZT of undoped LaBrI enhanced from ~ 0.48 to ~ 1.14 for up spin and from ~ 0.99 to ~ 1.12 for down spin with p-type doping. For the strained system highest ZT of ~ 1.92 at 800K for down spin with p-type doping is calculated. Computed ZT with 8% strain has significant improvement of ZT from ~ 1.51 to ~ 1.92 at 800K. Thus, for the studied Janus monolayer of LaBrI, ZT significantly increases from ~ 1 to ~ 1.92 with strain. Specifically, this monolayer showed the highest values of ~ 1.52 , ~ 1.73 , ~ 1.92 , and ~ 1.54 for 600K, 800K, 1200K, and 1500K respectively under the tensile strain of 8%. Also, the p-type doping is more favorable for enhancing the ZT values.

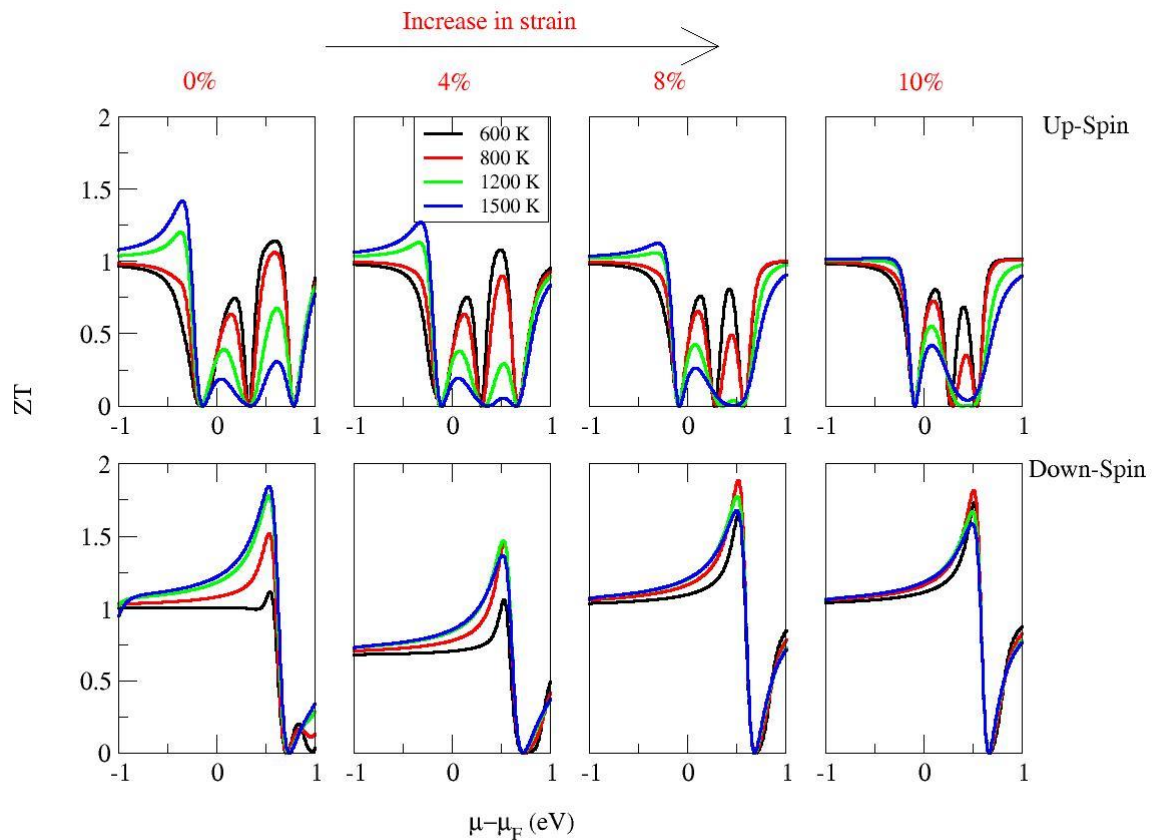


Figure 7: ZT as a function of chemical potential in different temperature regions.

Moreover, the studied Janus ferroelectric monolayer LaBrI exhibits higher ZT values which are prominent for potential thermoelectric materials.

Conclusions

We have systematically investigated the structural parameters of 2D Janus ferrovalley LaBrI material. Phonon dispersion curves at different strains revealed this material to be dynamically stable at 10% strain. The calculated electronic band structure signifies LaBrI to be an indirect band gap (0.54eV) ferromagnetic material with a magnetic moment of $1\mu_B$. Band gap with spin-up and spin-down charge carriers can be effectively modulated by biaxial tensile strain and it has a crucial impact on the thermoelectric transport properties. Computed thermoelectric coefficients suggest that this material can have a high power factor with n-type and p-type doping and low thermal conductivities of $\sim 1.03 \times 10^{14} W/mKs$ that results in high ZT ~ 1.92 at 800K at 8% strain. Thus, observed ZT >1 for strained systems which is comparable to the commercially used TE materials such as Bi_2Te_3 , oxides, sulphides makes this material to be a potential thermoelectric material. Overall, these results indicate that Janus monolayers of LaBrI can be a potential material for thermoelectric applications.

Acknowledgments

We would like to acknowledge the fellowship and computational resources provided by the Indian Statistical Institute, Kolkata, those have been helpful during this research. Also, we would like to acknowledge the developers of ELK code and Quantum espresso for providing free open-source codes.

References

- [1]. Ang, Tze-Zhang, Mohamed Salem, Mohamad Kamarol, Himadry Shekhar Das, Mohammad Alhuyi Nazari, and Natarajan Prabakaran. "A comprehensive study of renewable energy sources: Classifications, challenges, and suggestions." *Energy Strategy Reviews* **43**, 100939 (2022).
- [2]. Wehbi, Zahra, Rani Taher, Jalal Faraj, Cathy Castelain, and Mahmoud Khaled. "Hybrid thermoelectric generators-renewable energy systems: A short review on recent developments." *Energy Reports* **8**, 1361 (2022).
- [3]. Sasidharan, Manoj, Mohd Faizul Mohd Sabri, Sharifah Fatmadiana Wan Muhammad Hatta, and Suriani Ibrahim. "A review on the progress and development of thermoelectric air conditioning system." *International Journal of Green Energy* **21**, 283 (2024).
- [4]. Maleki, Reza, Mohsen Asadnia, and Amir Razmjou. "Artificial Intelligence-Based Material Discovery for Clean Energy Future." *Advanced Intelligent Systems* **10**, 2200073 (2022).

- [5]. Ma, Kun, Lingyu Xu, Azher M. Abed, Dalia H. Elkamchouchi, Mohamed Amine Khadimallah, H. Elhosiny Ali, H. Algarni, and Hamid Assilzadeh. "An artificial intelligence approach study for assessing hydrogen energy materials for energy saving in building." *Sustainable Energy Technologies and Assessments* **56**, 103052 (2023).
- [6]. Albert, Max DA, Katherine O. Bennett, Charlotte A. Adams, and Jon G. Gluyas. "Waste heat mapping: A UK study." *Renewable and Sustainable Energy Reviews* **160**, 112230 (2022).
- [7]. Farhat, Obeida, Jalal Faraj, Farouk Hachem, Cathy Castelain, and Mahmoud Khaled. "A recent review on waste heat recovery methodologies and applications: Comprehensive review, critical analysis, and potential recommendations." *Cleaner Engineering and Technology* **6**, 100387 (2022).
- [8]. Nandhini, Rajendran, Baskaran Sivaprakash, and Natarajan Rajamohan. "Waste heat recovery at low temperature from heat pumps, power cycles and integrated systems—Review on system performance and environmental perspectives." *Sustainable Energy Technologies and Assessments* **52**, 102214 (2022).
- [9]. Tian, Zhen, Zhixin Qi, Wanlong Gan, Molin Tian, and Wenzhong Gao. "A novel negative carbon-emission, cooling, and power generation system based on combined LNG regasification and waste heat recovery: Energy, exergy, economic, environmental (4E) evaluations." *Energy* **257**, 124528 (2022).
- [10]. Patel, Anand. "Advancements in heat exchanger design for waste heat recovery in industrial processes." *World Journal of Advanced Research and Reviews (WJARR)* **19**, 137 (2023).
- [11]. Kumari, Anuja, Abhinav Nag, and Jagdish Kumar. "Ab-initio study of halogen inter-substituted perovskite cesium leads halides for photovoltaic applications." *Journal of Physics and Chemistry of Solids* **161**, 110430 (2022).
- [12]. Olabi, A. G., Mohammed Al-Murisi, Hussein M. Maghrabie, Bashria AA Yousef, Enas Taha Sayed, Abdul Hai Alami, and Mohammad Ali Abdelkareem. "Potential applications of thermoelectric generators (TEGs) in various waste heat recovery systems." *International Journal of Thermofluids* **16**, 100249 (2022).
- [13]. Ge, Minghui, Zhenhua Li, Yuntong Zhao, Zhiwei Xuan, Yanzhe Li, and Yulong Zhao. "Experimental study of thermoelectric generator with different numbers of modules for waste heat recovery." *Applied Energy* **322**, 119523 (2022).
- [14]. Ochieng, Alfred Oloo, Tamer F. Megahed, Shinichi Ookawara, and Hamdy Hassan. "Comprehensive review in waste heat recovery in different thermal energy-consuming processes using thermoelectric generators for electrical power generation." *Process Safety and Environmental Protection* **162**, 134 (2022).
- [15]. Ma, Xiangrong, Shenhua Hu, Wuyuan Hu, Yuze Luo, and Hao Cheng. "Experimental investigation of waste heat recovery of thermoelectric generators with temperature gradient." *International Journal of Heat and Mass Transfer* **185**, 122342 (2022).

- [16]. Burnete, Nicolae Vlad, Florin Mariasiu, Christopher Depcik, Istvan Barabas, and Dan Moldovanu. "Review of thermoelectric generation for internal combustion engine waste heat recovery." *Progress in Energy and Combustion Science* **91**, 101009 (2022).
- [17]. Zhu, Sijing, Zheng Fan, Baoquan Feng, Runze Shi, Zexin Jiang, Ying Peng, Jie Gao, Lei Miao, and Kunihito Koumoto. "Review on wearable thermoelectric generators: from devices to applications." *Energies* **15**, 3375 (2022).
- [18]. Liu, Yuming, Jordi-Roger Riba, Manuel Moreno-Eguilaz, and Joseo Sanllehi. "Application of Thermoelectric generators for low temperature gradient energy harvesting." *Applied Science* **13**, 2603 (2023).
- [19]. Newby, Samantha, Wajira Mirihanage, and Anura Fernando. "Recent advancements in thermoelectric generators for smart textile application." *Materials Today Communications* **33**, 104585 (2022).
- [20]. Jabri, Milad, Saeed Masoumi, Fahimehsadat Sajadirad, Roger P. West, and Amir Pakdel. "Thermoelectric Energy Conversion in Buildings." *Materials Today Energy* **32**, 101257 (2023).
- [21]. Zoui, Mohamed Amine, Saïd Bentouba, John G. Stocholm, and Mahmoud Bourouis. "A review on thermoelectric generators: Progress and applications." *Energies* **13**, 3606 (2020).
- [22]. Nag, Abhinav, Yuhit Gupta, and Jagdish Kumar. "Spin-polarized linear dispersions, lattice dynamics and transport properties of quaternary Heusler alloys (LiMgXSb)." *Materials Chemistry and Physics* **297**, 127373 (2023).
- [23]. Ma, Qianli, Haisheng Fang, and Mengjie Zhang. "Theoretical analysis and design optimization of thermoelectric generator." *Applied Thermal Engineering* **127**, 758 (2017).
- [24]. McCarty, R. "Thermoelectric power generator design for maximum power: it's all about ZT." *Journal of electronic materials* **42**, 1504 (2013).
- [25]. Pennelli, Giovanni, Elisabetta Dimaggio, and Massimo Macucci. "Electrical and thermal optimization of energy-conversion systems based on thermoelectric generators." *Energy* **240**, 122494 (2022).
- [26]. Tuley, Richard, and Kevin Simpson. "ZT optimization: an application focus." *Materials* **10**, 309 (2017).
- [27]. Wei, Jiangtao, Liangliang Yang, Zhe Ma, Peishuai Song, Mingliang Zhang, Jing Ma, Fuhua Yang, and Xiaodong Wang. "Review of current high-ZT thermoelectric materials." *Journal of Materials Science* **55**, 12642 (2020).
- [28]. Wolf, Mario, Richard Hinterding, and Armin Feldhoff. "High power factors vs. high zT- A review of thermoelectric materials for high-temperature application." *Entropy* **21**, 1058 (2019).
- [29]. Ma, Zhe, Jiangtao Wei, Peishuai Song, Mingliang Zhang, Liangliang Yang, Jing Ma, Wen Liu, Fuhua Yang, and Xiaodong Wang. "Review of experimental approaches for

- improving ZT of thermoelectric materials." *Materials Science in Semiconductor Processing* **121**, 105303 (2021).
- [30]. Hasan, Md Nazibul, Herman Wahid, Nafarizal Nayan, and Mohamed Sultan Mohamed Ali. "Inorganic thermoelectric materials: A review." *International Journal of Energy Research* **44**, 6170 (2020).
- [31]. Liu, Wei-Di, De-Zhuang Wang, Qingfeng Liu, Wei Zhou, Zongping Shao, and Zhi-Gang Chen. "High-performance GeTe-based thermoelectrics: from materials to devices." *Advanced Energy Materials* **10**, 2000367 (2020).
- [32]. Cai, Bowen, Haihua Hu, Hua-Lu Zhuang, and Jing-Feng Li. "Promising materials for thermoelectric applications." *Journal of Alloys and Compounds* **806**, 471 (2019).
- [33]. Sakane, Shunya, Takafumi Ishibe, Tatsuhiko Taniguchi, Nobuyasu Naruse, Yutaka Mera, Takeshi Fujita, Md Mahfuz Alam, Kentarou Sawano, Nobuya Mori, and Yoshiaki Nakamura. "Thermoelectric power factor enhancement based on carrier transport physics in ultimately phonon-controlled Si nanostructures." *Materials Today Energy* **13**, 56 (2019).
- [34]. Xu, Rui, Lulu Huang, Jian Zhang, Di Li, Jizi Liu, Jiang Liu, Jun Fang, Meiyu Wang, and Guodong Tang. "Nanostructured SnSe integrated with Se quantum dots with ultrahigh power factor and thermoelectric performance from magnetic field-assisted hydrothermal synthesis." *Journal of Materials Chemistry A* **7**, 15757 (2019).
- [35]. Murmu, Peter P., Varun Karthik, Zihang Liu, Vedran Jovic, Takao Mori, Wanli L. Yang, Kevin E. Smith, and John V. Kennedy. "Influence of carrier density and energy barrier scattering on a high Seebeck coefficient and power factor in transparent thermoelectric copper iodide." *ACS Applied Energy Materials* **3**, 10037 (2020).
- [36]. Liu, Zihang, Xianfu Meng, Dandan Qin, Bo Cui, Haijun Wu, Yang Zhang, Stephen J. Pennycook, Wei Cai, and Jiehe Sui. "New insights into the role of dislocation engineering in N-type filled skutterudite CoSb₃." *Journal of Materials Chemistry C* **7**, 13622 (2019).
- [37]. Guan, Xin, Wei Feng, Xizu Wang, Roshani Venkatesh, and Jianyong Ouyang. "Significant enhancement in the Seebeck coefficient and power factor of p-type poly (3, 4-ethylenedioxythiophene): poly (styrenesulfonate) through the incorporation of n-type MXene." *ACS applied materials & interfaces* **12**, 13013 (2020).
- [38]. Tolborg, Kasper, and Bo B. Iversen. "Chemical bonding origin of the thermoelectric power factor in half-Heusler semiconductors." *Chem. Mater* **33**, 5308 (2021).
- [39]. Dylla, Maxwell T., Jimmy Jiahong Kuo, Ian Witting, and Gerald Jeffrey Snyder. "Grain boundary engineering nanostructured SrTiO₃ for thermoelectric applications." *Advanced Materials Interfaces* **6**, 1900222 (2019).
- [40]. Zhao, Ting, Huaxing Zhu, Bin Zhang, Sikang Zheng, Nanhai Li, Guiwen Wang, Guoyu Wang, Xu Lu, and Xiaoyuan Zhou. "High thermoelectric performance of tellurium-free n-type AgBi_{1-x}Sb_xSe₂ with stable cubic structure enabled by entropy engineering." *Acta Materialia* **220**, 117291 (2021).

- [41]. Wei, Jiangtao, Liangliang Yang, Zhe Ma, Peishuai Song, Mingliang Zhang, Jing Ma, Fuhua Yang, and Xiaodong Wang. "Review of current high-ZT thermoelectric materials." *Journal of Materials Science* **55**, 12642 (2020).
- [42]. He, Allan, Sabah K. Bux, Yufei Hu, David Uhl, Li Li, Davide Donadio, and Susan M. Kauzlarich. "Structural complexity and high thermoelectric performance of the Zintl phase: Yb₂₁Mn₄Sb₁₈." *Chemistry of Materials* **31**, 8076 (2019).
- [43]. Zhang, Xiwen, Yilv Guo, Zhaobo Zhou, Yunhai Li, Yunfei Chen, and Jinlan Wang. "A general strategy for designing two-dimensional high-efficiency layered thermoelectric materials." *Energy & Environmental Science* **14**, 4059 (2021).
- [44]. Lai, Huajun, Ying Peng, Jie Gao, Masashi Kurosawa, Osamu Nakatsuka, Tsunehiro Takeuchi, and Lei Miao. "Silicon-based low-dimensional materials for thermal conductivity suppression: Recent advances and new strategies to high thermoelectric efficiency." *Japanese Journal of Applied Physics* **60**, SA0803 (2020).
- [45]. Jung, Young-Kwang, In Taek Han, Yong Churl Kim, and Aron Walsh. "Prediction of high thermoelectric performance in the low-dimensional metal halide Cs₃Cu₂I₅." *npj Computational Materials* **7**, 51 (2021).
- [46]. Huang, Si-Zhao, Qing-Yi Feng, Bi-Yi Wang, Hong-Dong Yang, Bo Li, Xia Xiang, Xiaotao Zu, and Hong-Xiang Deng. "Valley Degeneracy-Enhanced Thermoelectric Performance in In-Based FeOCl-Type Monolayers." *ACS Applied Energy Materials* **5**, 13042 (2022).
- [47]. Guo, Zhe, Qiang Zhang, Hongxiang Wang, Xiaojian Tan, Fanfan Shi, Chenglong Xiong, Na Man, Haoyang Hu, Guoqiang Liu, and Jun Jiang. "Bi-Zn codoping in GeTe synergistically enhances band convergence and phonon scattering for high thermoelectric performance." *Journal of Materials Chemistry A* **8**, 21642 (2020).
- [48]. Zong, Peng-an, Jia Liang, Peng Zhang, Chunlei Wan, Yifeng Wang, and Kunihiro Koumoto. "Graphene-based thermoelectrics." *ACS Applied Energy Materials* **3**, 2224 (2020).
- [49]. Markov, Maxime, and Mona Zebarjadi. "Thermoelectric transport in graphene and 2D layered materials." *Nanoscale and Microscale Thermophysical Engineering* **23**, 117 (2019).
- [50]. Zhu, Xue-Liang, Hengyu Yang, Wu-Xing Zhou, Baotian Wang, Ning Xu, and Guofeng Xie. "KAgX (X= S, Se): high-performance layered thermoelectric materials for medium-temperature applications." *ACS applied materials & interfaces* **12**, 36102 (2020).
- [51]. Zhang, Xiwen, Chenhan Liu, Yi Tao, Yunhai Li, Yilv Guo, Yunfei Chen, Xiao Cheng Zeng, and Jinlan Wang. "High ZT 2D Thermoelectrics by Design: Strong Interlayer Vibration and Complete Band-Extrema Alignment." *Advanced Functional Materials* **30**, 2001200 (2020).
- [52]. Sarikurt, Sevil, Tuğbey Kocabaş, and Cem Sevik. "High-throughput computational screening of 2D materials for thermoelectrics." *Journal of Materials Chemistry A* **8**, 19674 (2020).

- [53]. Zhu, Zhili, Xiaolin Cai, Seho Yi, Jinglei Chen, Yawei Dai, Chunyao Niu, Zhengxiao Guo et al. "Multivalency-driven formation of Te-based monolayer materials: a combined first-principles and experimental study." *Physical review letters* **119**, 106101 (2017).
- [54]. Zhu, Beibei, Qichao Chen, Siyao Jiang, Milo Holt, Weinan Zhu, Deji Akinwande, and Li Tao. "Thermoelectric effect and devices on IVA and VA Xenos." *InfoMat* **3**, 271 (2021).
- [55]. Yuan, Junjie, Guowei Liu, Yi Xin, Xinyu Wang, Yiping Liu, Xue Han, Shenggui Fu, Zhongsheng Man, Fei Xing, and Fang Zhang. "Synthetic 2D tellurium nanosheets with intense TE wave polarization absorption by employing the PVD method." *Journal of Nanoparticle Research* **24**, 130 (2022).
- [56]. Kim, Jeongmin, Seonhye Youn, Joonho Bang, Hongjae Moon, Woosun Jang, Jong Wook Roh, Dong Hwan Kim, Joonyeon Chang, and Wooyoung Lee. "Experimental verification of semimetallic band structure in PtSe₂ via thermoelectric power measurements." *Applied Physics Letters* **120**, 043103 (2022).
- [57]. Gu, Xiaokun, and Ronggui Yang. "Phonon transport in single-layer transition metal dichalcogenides: A first-principles study." *Applied Physics Letters* **105**, 131903 (2014).
- [58]. Li and his co-workers synthesized MoSSe Janus monolayer experimentally using CVD technique in 2017 [Li, Ruiping, Yingchun Cheng, and Wei Huang. "Recent progress of Janus 2D transition metal chalcogenides: from theory to experiments." *Small* **14**, 1802091 (2018).
- [59]. Kumari, Anuja, Abhinav Nag, and Jagdish Kumar. "Strain engineering and thermoelectric performance of Janus monolayers of titanium dichalcogenides: A DFT study." *Computational Materials Science* **218**, 111925 (2023).
- [60]. Patel, Abhishek, Deobrat Singh, Yogesh Sonvane, P. B. Thakor, and Rajeev Ahuja. "High thermoelectric performance in two-dimensional Janus monolayer material WS-X (X= Se and Te)." *ACS applied materials & interfaces* **12**, 46212 (2020).
- [61]. Huang, Si-Zhao, Cheng-Ge Fang, Qing-Yi Feng, Bi-Yi Wang, Hong-Dong Yang, Bo Li, Xia Xiang, Xiao-Tao Zu, and Hong-Xiang Deng. "Strain Tunable Thermoelectric Material: Janus ZrSSe Monolayer." *Langmuir* **39**, 2719 (2023).
- [62]. Tao, Wang-Li, Jun-Qing Lan, Cui-E. Hu, Yan Cheng, Jun Zhu, and Hua-Yun Geng. "Thermoelectric properties of Janus MXY (M= Pd, Pt; X, Y= S, Se, Te) transition-metal dichalcogenide monolayers from first principles." *Journal of Applied Physics* **127**, 035101 (2020).
- [63]. Saini, Shivani, Anup Shrivastava, Ambesh Dixit, and Sanjai Singh. "Ultra-low lattice thermal conductivity and high figure of merit for Janus MoSeTe monolayer: a peerless material for high temperature regime thermoelectric devices." *Journal of Materials Science* **57**, 7012 (2022).
- [64]. Sattar, Shahid, Md Fhokrul Islam, and Carlo M. Canali. "Monolayer Mn X and Janus X Mn Y (X, Y= S, Se, Te): A family of two-dimensional antiferromagnetic semiconductors." *Physical Review B* **106**, 085410 (2022).

- [65]. Wu, Daoxiong, Zhiwen Zhuo, Haifeng Lv, and Xiaojun Wu. "Two-dimensional Cr₂X₃S₃ (X= Br, I) Janus semiconductor with intrinsic room-temperature magnetism." *The Journal of Physical Chemistry Letters* **12**, 2905 (2021).
- [66]. Jiang, Peng, Lili Kang, Yan-Ling Li, Xiaohong Zheng, Zhi Zeng, and Stefano Sanvito. "Prediction of the two-dimensional Janus ferrovalley material LaBrI." *Physical Review B* **104**, 035430 (2021).
- [67]. Chaurasiya, Rajneesh, Shubham Tyagi, Nirpendra Singh, Sushil Auluck, and Ambesh Dixit. "Enhancing thermoelectric properties of Janus WSSe monolayer by inducing strain mediated valley degeneracy." *Journal of Alloys and Compounds* **855**, 157304 (2021).
- [68]. K. Dewhurst, S. Sharma, L. Nordstrom, F. Cricchio, F. Bultmark, H. Gross, C. Ambrosch-Draxl, ELK, <http://elk.sourceforge.net> (2016).
- [69]. Giannozzi, Paolo, Stefano Baroni, Nicola Bonini, Matteo Calandra, Roberto Car, Carlo Cavazzoni, Davide Ceresoli et al. "QUANTUM ESPRESSO: a modular and open-source software project for quantum simulations of materials." *Journal of physics: Condensed matter* **21**, 395502 (2009).
- [70]. Perdew, John P., Kieron Burke, and Matthias Ernzerhof. "Generalized gradient approximation made simple." *Physical review letters* **77**, 3865 (1996).
- [71]. Madsen, Georg KH, and David J. Singh. "BoltzTraP. A code for calculating band-structure dependent quantities." *Computer Physics Communications* **175**, 67 (2006).
- [72]. Nag, Abhinav, and Jagdish Kumar. "Dirac dispersions, lattice dynamics and thermoelectric properties of quaternary Heusler alloys LiMgXY (X= Pt, Pd, Au; Y= Sb, Sn)." *Materials Today Communications* **31**, 103400 (2022).
- [73]. J. Mao, H. Zhu, Z. Ding, Z. Liu, G.A. Gamage, G. Chen, Z. Ren, High thermoelectric cooling performance of n-type Mg₃Bi₂-based materials, *Science* **365**, 495 (2019).
- [74]. Nag, Abhinav, Anuja Kumari, and Jagdish Kumar. "Revisiting Wiedemann-Franz law through Boltzmann transport equations and ab-initio density functional theory." *AIP Conference Proceedings*. **1953**, 1 (2018).